Supplementary Information

Bacillus-derived nelfinavir and octyl gallate block PRRSV replication via modulating its lipid remodeling

Haiyan Wang[a,b,c], Wenwu Jiang[a,b,c], Xiaoya Mo[a,b,c], Yawei Sun[a,b,c], Mingxing Lu[a,b,c], Shudan Liu[a,b,c], Chao Zhang[a,b,c], Xiaochao Duan[a,b,c], Feifan Zhao[a,b,c], Xinxin Li [a,b,c*], Xiangmin Li[a,b,c,d*], Ping Qian[a,b,c,d*]

[a]National Key Laboratory of Agricultural Microbiology, Hubei Hongshan Laboratory, Huazhong Agricultural University, Wuhan 430070, Hubei, PRC

[b]College of Veterinary Medicine, Huazhong Agricultural University, Wuhan, 430070, Hubei, PRC

[c]Key Laboratory of Preventive Veterinary Medicine in Hubei Province, The Cooperative Innovation Center for Sustainable Pig Production, Wuhan, 430070, Hubei, PRC

[d]Hubei Jiangxia Laboratory, Wuhan, 430200, PRC.

* Correspondence: lixinxin@mail.hzau.edu.cn (X. Li); lixiangmin@mail.hzau.edu.cn (X. Li); qianp@mail.hzau.edu.cn (P. Qian)

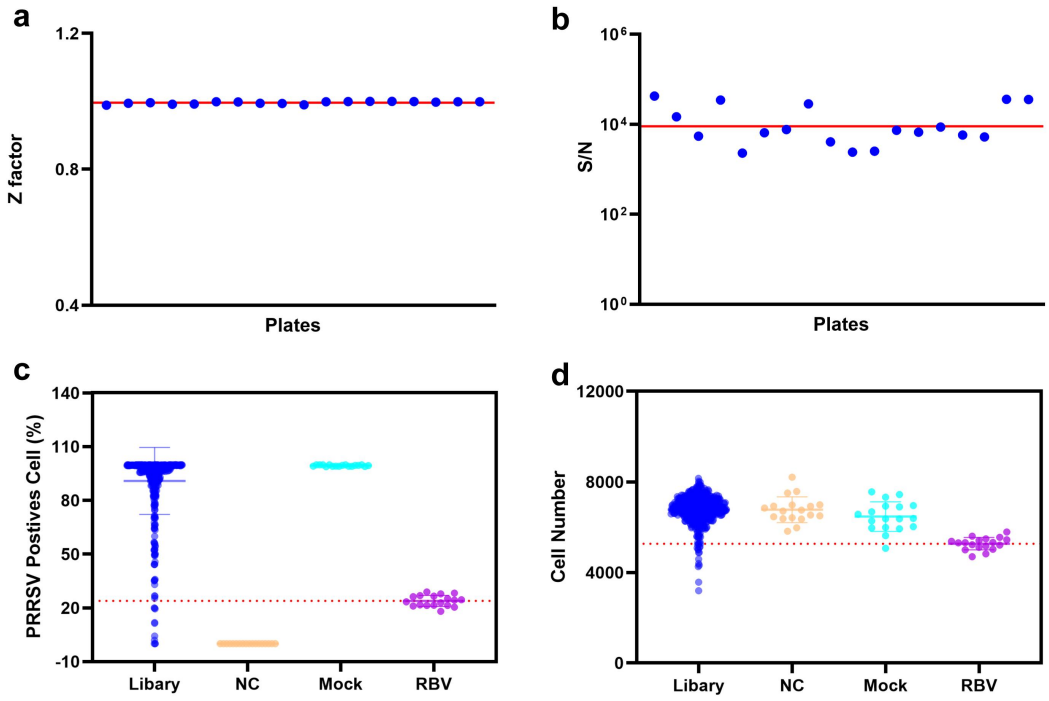

Supplementary Fig. 1 Quality control metrics for the HTS assay used to screen anti-PRRSV *Bacillus* fermentation-broth preparations.

(a) Z'-factor values for the 18 screening plates.

(b) Signal-to-noise (S/N) ratios for the 18 screening plates.

(c) Percentages of PRRSV-positive cells in the indicated groups.

(d) Cell numbers per well in the indicated groups.

Red lines indicate the thresholds used for assay performance evaluation and hit selection.

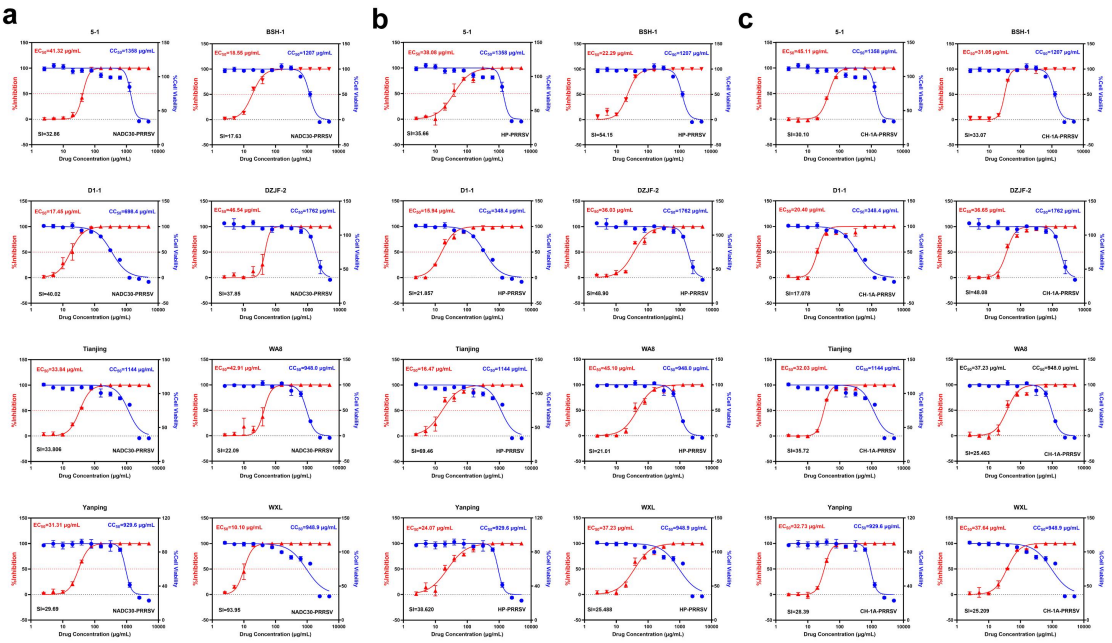

Supplementary Fig. 2. Antiviral activities of fermentation-broth preparations from eight *Bacillus* strains against distinct PRRSV strains.

Antiviral dose–response curves (red) and cytotoxicity curves (blue) of the indicated fermentation-broth preparations were determined in MARC-145 cells. EC_{50} and CC_{50} values are indicated in each panel. (a) NADC30-PRRSV; (b) HP-PRRSV; (c) CH-1A-PRRSV.

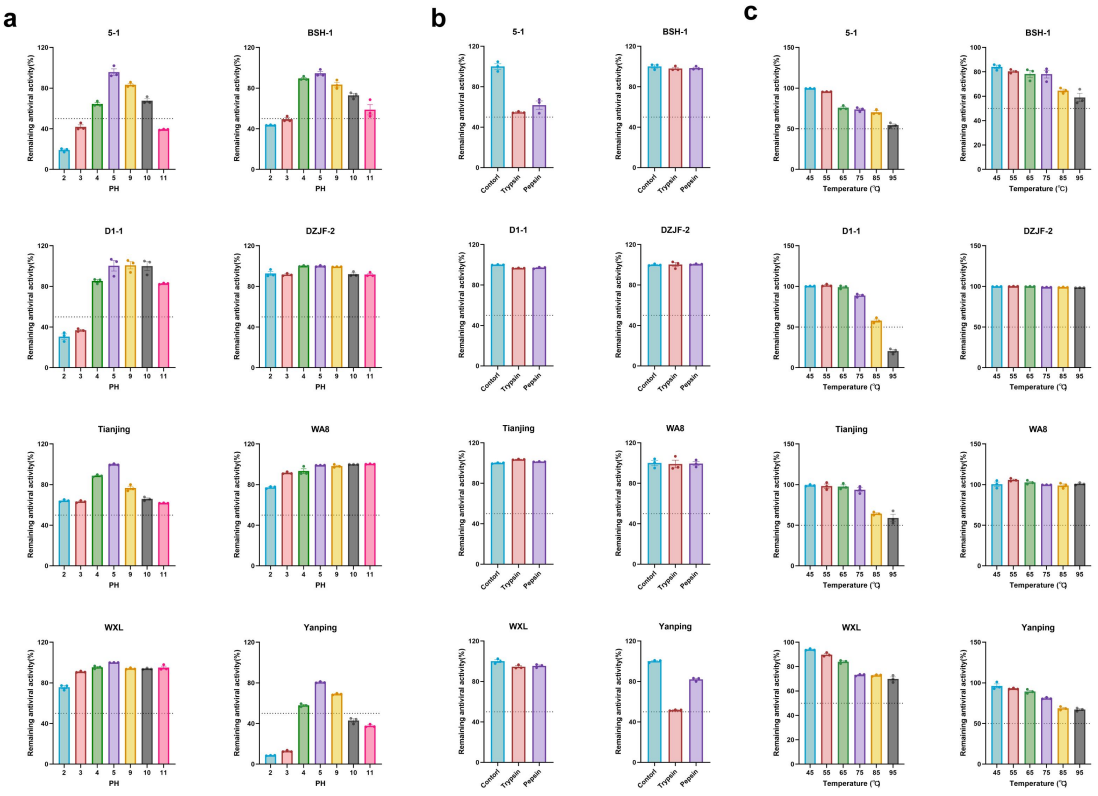

Supplementary Fig. 3: Stability of metabolites from eight *Bacillus* fermentation-broth preparations.

(a) Effect of pH on antiviral activity.

(b) Effect of digestive enzymes on antiviral activity.

(c) Effect of temperature on antiviral activity.

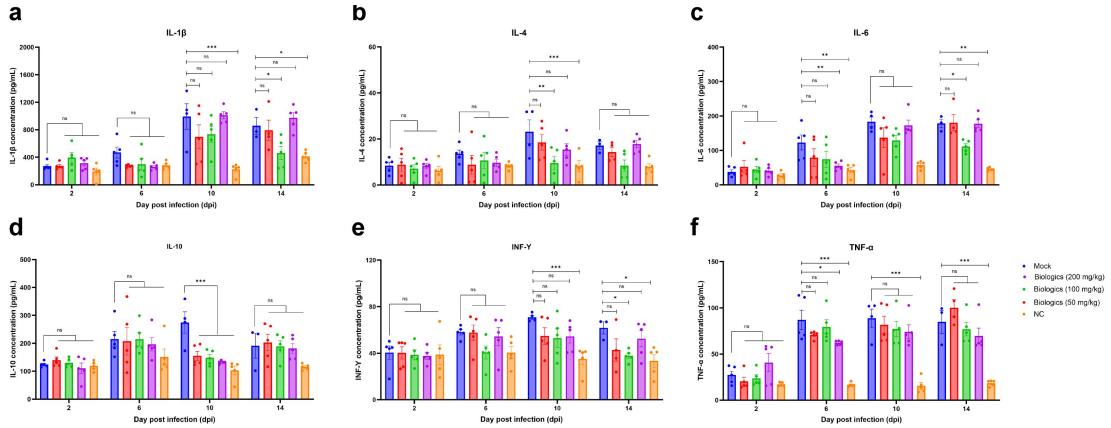

Supplementary Fig. 4: Effects of *Bacillus* fermentation-broth preparations treatment on serum cytokine levels in PRRSV-infected piglets.

Serum levels of IL-1β (a), IL-4 (b), IL-6 (c), IL-10 (d), IFN-γ (e) and TNF-α (f) were measured by ELISA at the indicated days post infection.

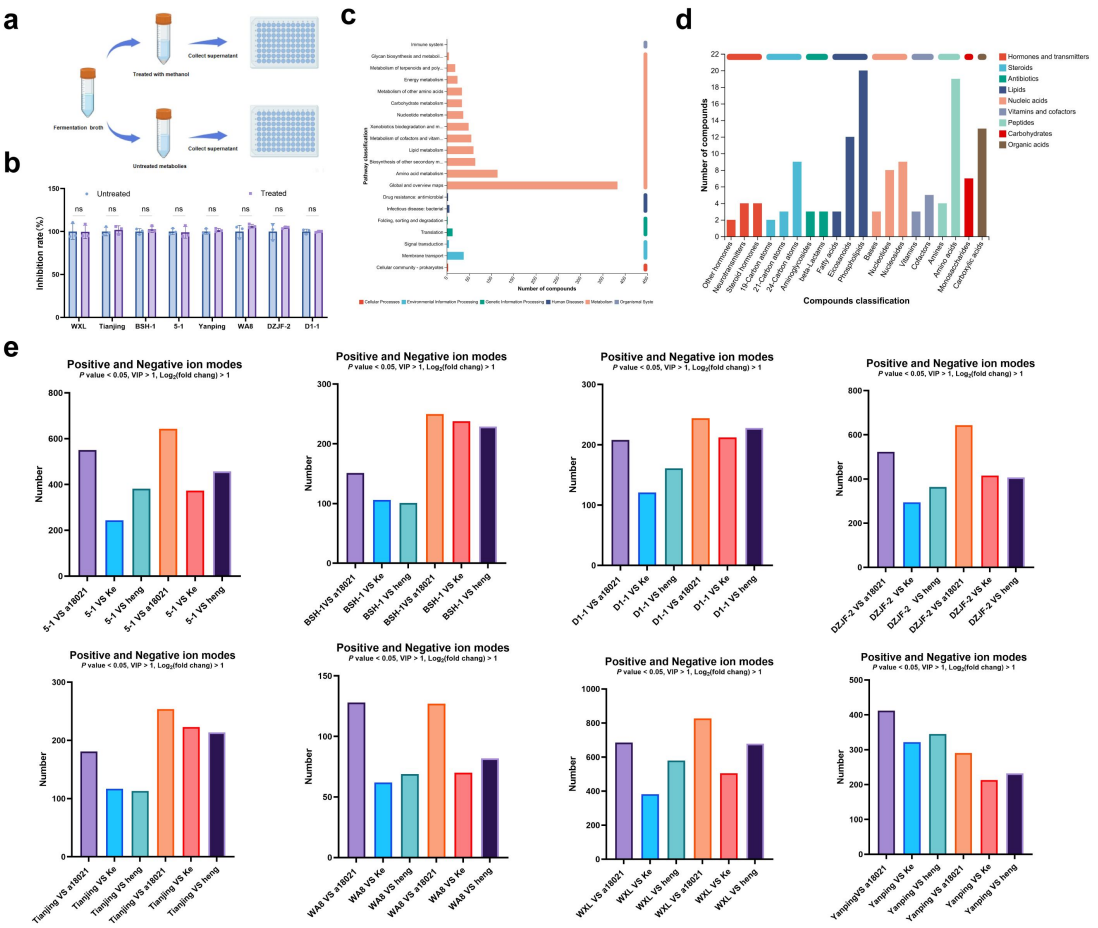

Supplementary Fig.5: Metabolomic screening of anti-PRRSV small molecules from *Bacillus* fermentation-broth preparations.

(a) Schematic of the workflow used for methanol treatment and metabolite preparation from the fermentation broths of eight *Bacillus* strains.

(b) Antiviral activities of untreated and methanol-treated broths, evaluated by the inhibition rate calculated from PRRSV genomic copies.

(c) KEGG pathway enrichment analysis of differential metabolites.

(d) Compound classification of differential metabolites.

(e) Numbers of differential small molecules identified in positive and negative ion modes for each antiviral *Bacillus* strain relative to non-antiviral strains, using the thresholds $P < 0.05$, VIP > 1 and $|\log_2 \text{(fold change)}| > 1$.

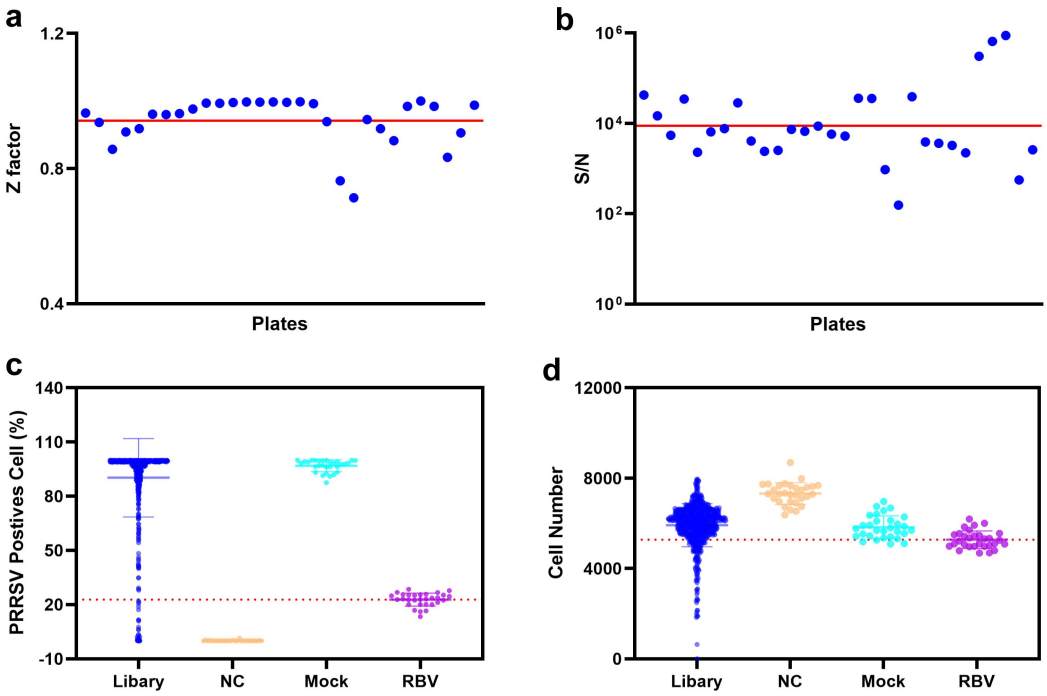

Supplementary Fig. 6: Quality control metrics for the HTS assay used to screen anti-PRRSV small-molecule metabolites.

(a) Z′-factor values for all 30 screening plates.

(b) Signal-to-noise ratios for all 30 screening plates.

(c) Percentages of PRRSV-positive cells in the indicated groups.

(d) Cell numbers in the indicated groups.

Red lines indicate the cutoff values used for assay performance evaluation and hit selection.

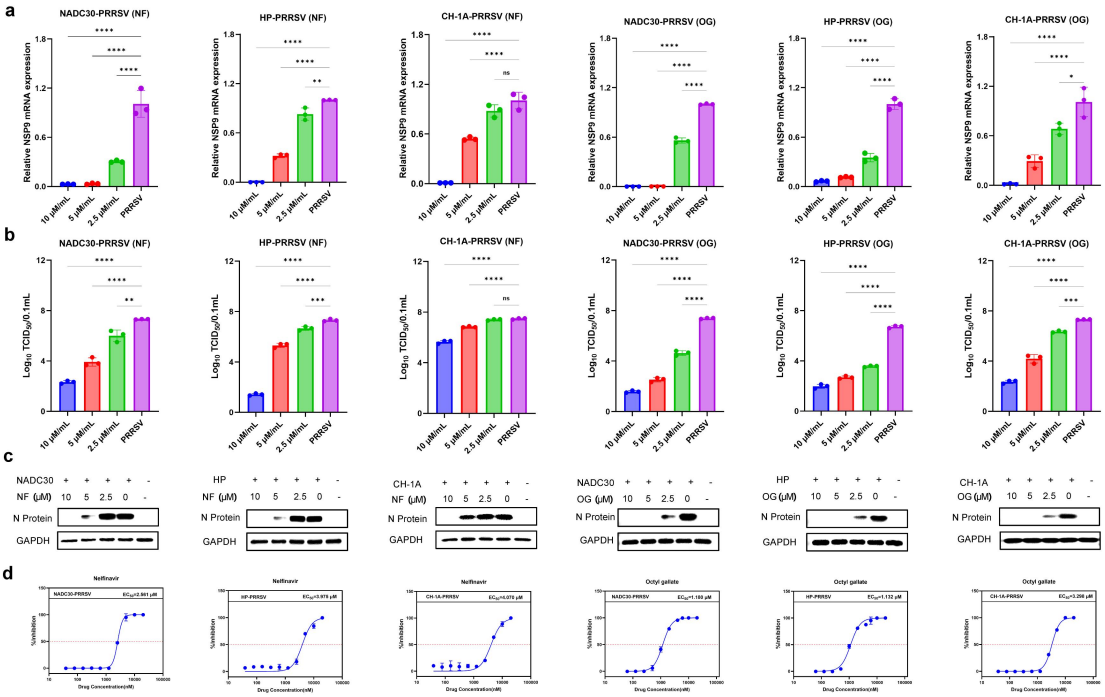

Supplementary Fig.7: Broad-spectrum antiviral activities of nelfinavir (NF) and octyl gallate (OG) against multiple PRRSV strains.

(a) Dose-dependent inhibition of viral RNA expression by NF and OG, measured by RT–qPCR analysis of NSP9 mRNA.

(b) Dose-dependent reduction in viral titers following NF or OG treatment.

(c) Western blot analysis of viral N protein expression in cells treated with the indicated concentrations of NF or OG.

(d) Dose–response curves and EC_{50} values of NF and OG against different PRRSV strains.

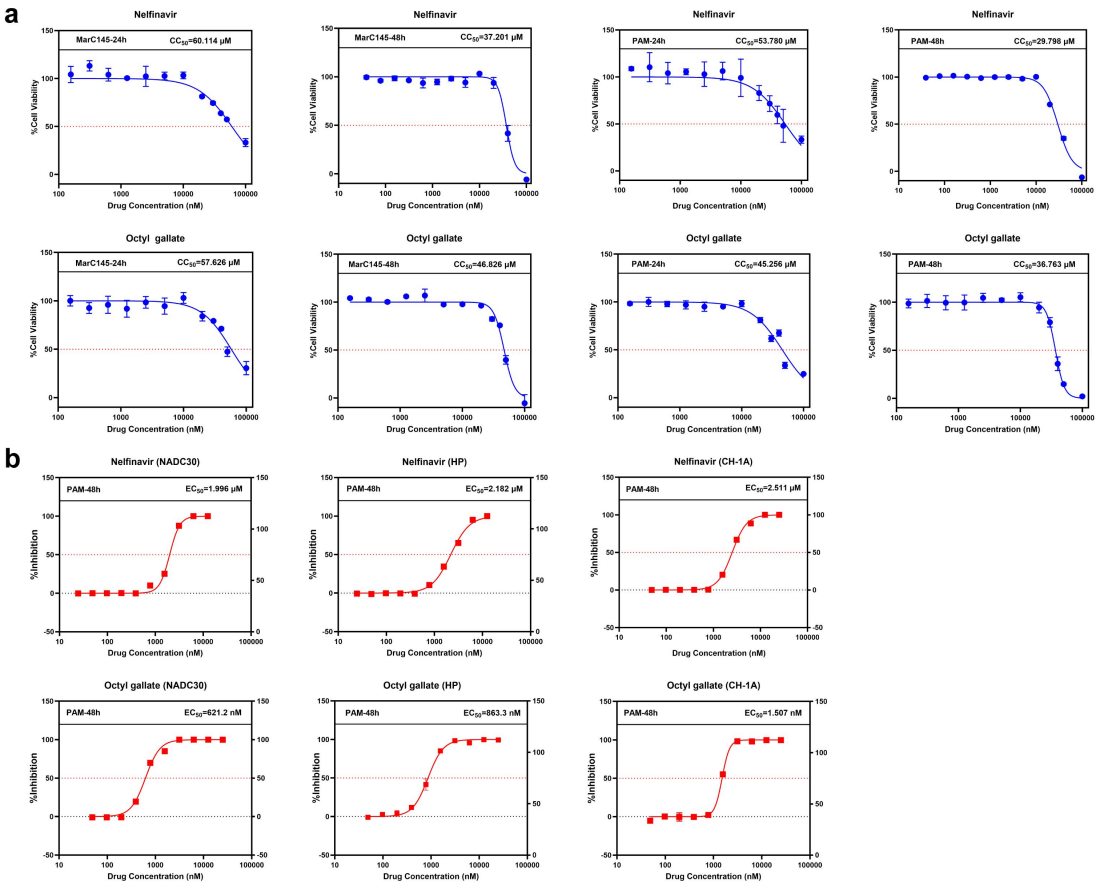

Supplementary Fig.8 CC_{50} and EC_{50} of NF and OG.

(a) Cytotoxicity of NF and OG in MARC-145 cells and PAMs after 24 h or 48 h of treatment, as determined by CCK-8 assays. Cell viability was normalized to the vehicle-treated control, and CC_{50} values were calculated from dose–response curves.

(b) Dose–response analysis of the antiviral activity of NF and OG against representative PRRSV strains, including NADC30-PRRSV, HP-PRRSV and CH-1A-PRRSV, in PAMs. Antiviral activity was calculated as the percentage inhibition of PRRSV infection relative to infected controls.

Dose–response curves were fitted by nonlinear regression

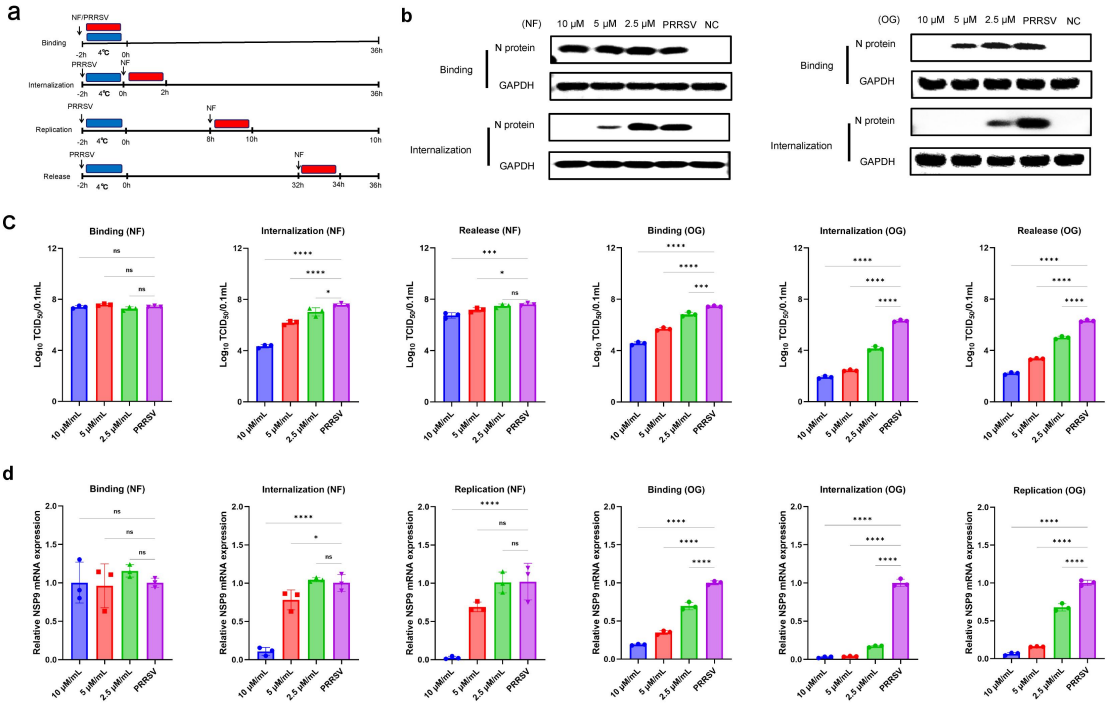

Supplementary Fig.9: Time-of-addition analysis of the anti-PRRSV activities of NF and OG.

(a) Schematic diagram of the time-of-addition assay used to evaluate the effects of NF and OG on PRRSV binding, internalization, replication and release. MARC-145 cells were infected with PRRSV-GFP (MOI = 1), and compounds were added at the indicated stages.

(b) Western blot analysis of PRRSV N protein expression after NF or OG treatment during the binding and internalization stages.

(c) Viral titers determined by $TCID_{50}$ assay after NF or OG treatment during the binding, internalization and release stages.

(d) Relative NSP9 mRNA levels measured by RT–qPCR after NF or OG treatment during the binding, internalization and replication stages.

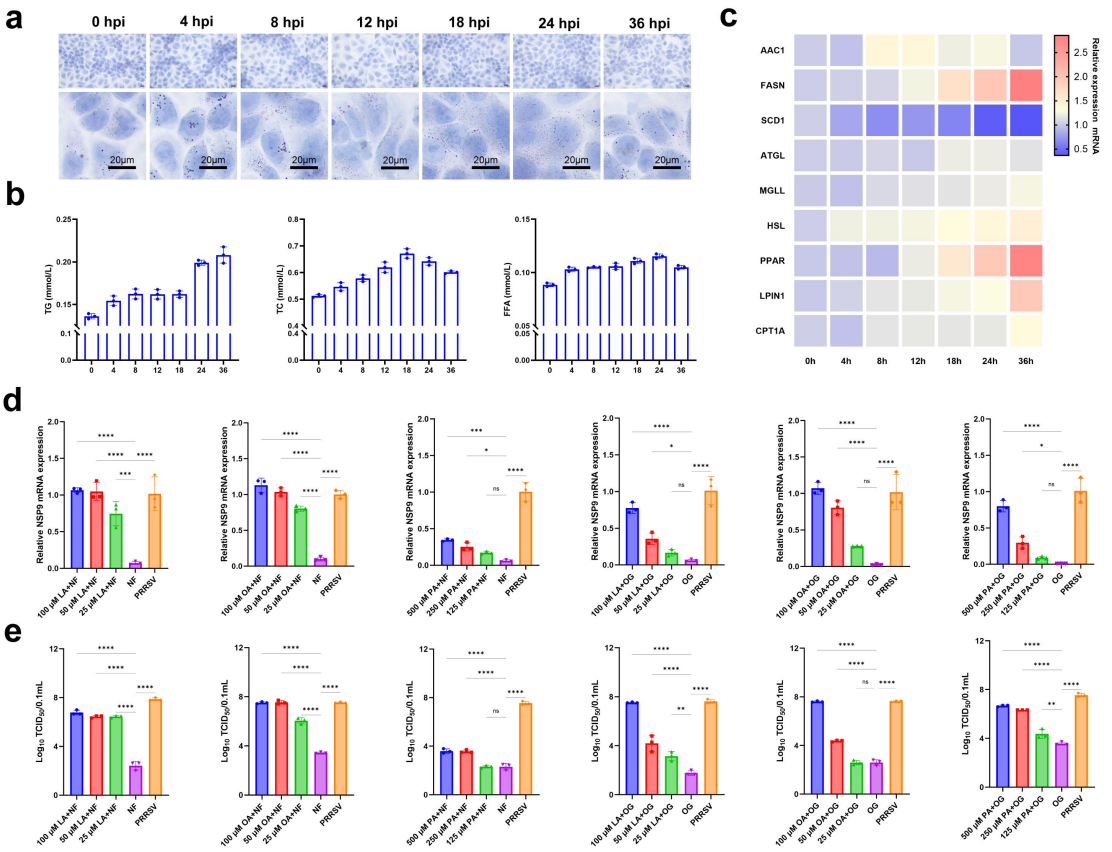

Supplementary Fig.10: PRRSV infection remodels lipid metabolism in MARC-145 cells.

(a) Representative images showing temporal changes in lipid droplet accumulation in PRRSV-infected MARC-145 cells at the indicated time points post-infection (MOI = 1). Scale bars, 20 μm.

(b) Dynamic changes in intracellular free fatty acid (FFA), total cholesterol (TC) and triglyceride (TG) levels in PRRSV-infected MARC-145 cells.

(c) Heatmap showing temporal changes in the mRNA expression of lipid metabolism-related genes in MARC-145 cells during PRRSV infection.

(d and e) Exogenous supplementation with linoleic acid (LA), oleic acid (OA) or palmitic acid (PA) at the indicated concentrations reversed the inhibitory effects of NF or OG on viral replication, as determined by RT–qPCR analysis of NSP9 mRNA levels (d) and viral titration (e) in PRRSV-infected MARC-145 cells.

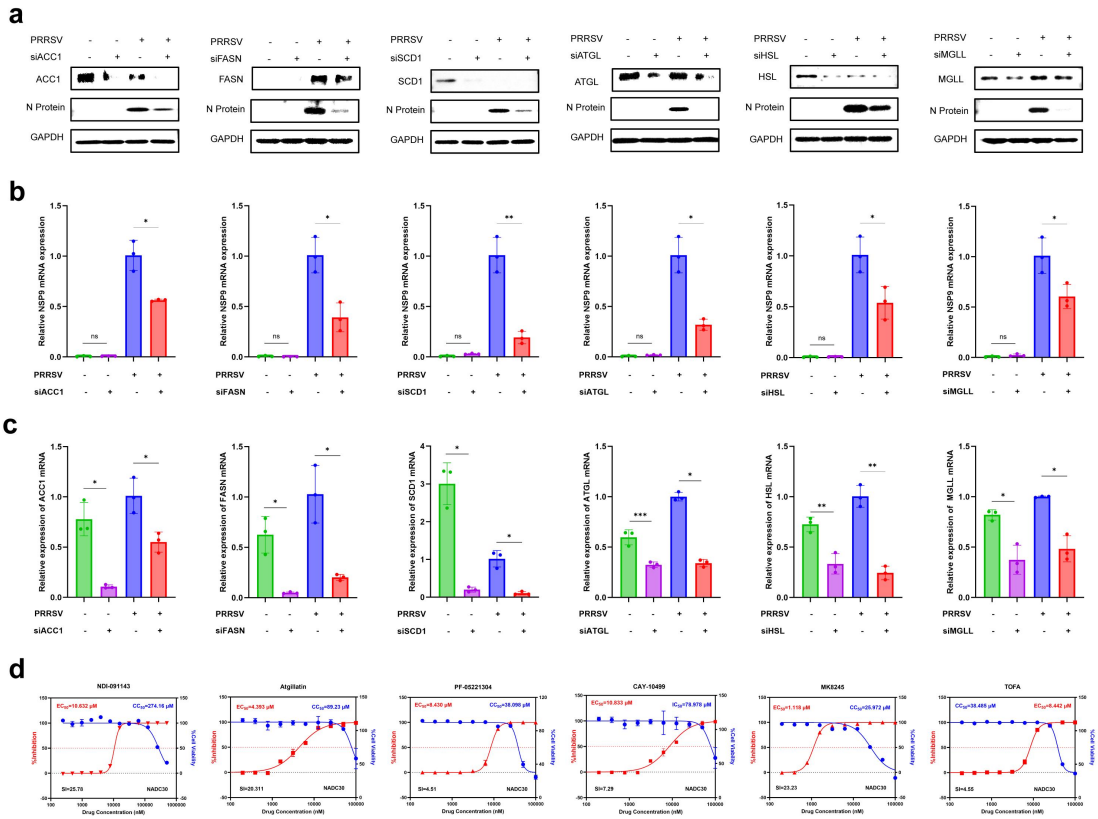

Supplementary Fig.11: PRRSV replication depends on host lipogenesis and lipolysis.

(a) Immunoblot analysis of PRRSV N protein expression in PRRSV-infected MARC-145 cells after siRNA-mediated knockdown of representative lipogenic genes (ACC1, FASN and SCD1) or lipolysis-associated genes (ATGL, HSL and MGLL). GAPDH was used as a loading control.

(b and c) RT–qPCR analysis showing that knockdown of these lipid metabolism-related genes reduced PRRSV NSP9 mRNA levels (b). The corresponding host genes were analysed in parallel to confirm knockdown efficiency (c).

(d) Dose–response analysis of antiviral activity and cytotoxicity for pharmacological inhibitors targeting lipid metabolic pathways. EC_{50} and CC_{50} values were calculated from fitted dose–response curves.

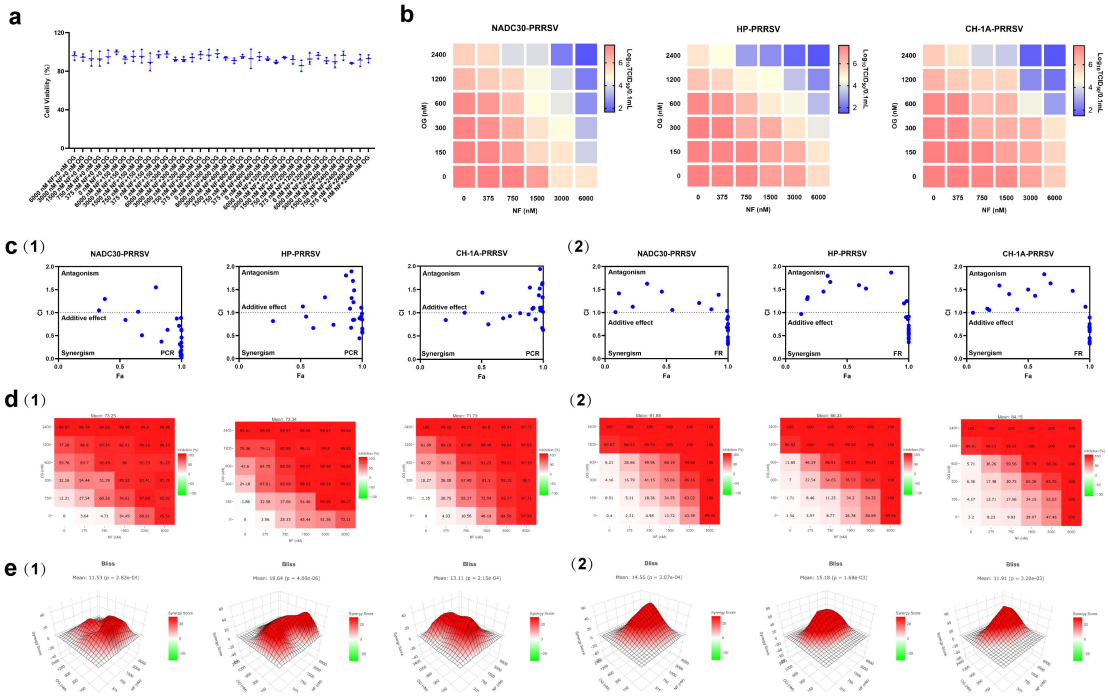

Supplementary Fig.12: Synergistic antiviral activity of NF and OG against PRRSV.

(a) Cell viability of MARC-145 cells treated with the indicated combinations of NF and OG.

(b) $TCID_{50}$-based antiviral activity of NF–OG combinations against NADC30-PRRSV, HP-PRRSV and CH-1A-PRRSV. NF concentrations (nM) are shown on the x axis and OG concentrations (nM) on the y axis; viral titres are indicated by the colour scale.

(c) CompuSyn analysis of the interaction between NF and OG. Fa–CI plots for the indicated PRRSV strains. CI < 1, CI = 1 and CI > 1 indicate synergistic, additive and antagonistic effects, respectively.

(d) Two-dimensional response matrices showing the antiviral effects of NF–OG combinations across the indicated dose ranges.

(e) Three-dimensional Bliss synergy landscapes of NF–OG combinations for the indicated PRRSV strains. Bliss scores > 10 indicate synergism, scores between −10 and 10 indicate additive effects, and scores < −10 indicate antagonism. Darker red regions indicate stronger synergistic effects.

For c–e, analyses labelled (1) were based on NSP9 RT–qPCR inhibition, whereas analyses labelled (2) were based on fluorescence-based infection inhibition. Panel c was generated using CompuSyn, and panels d and e were analysed using SynergyFinder.

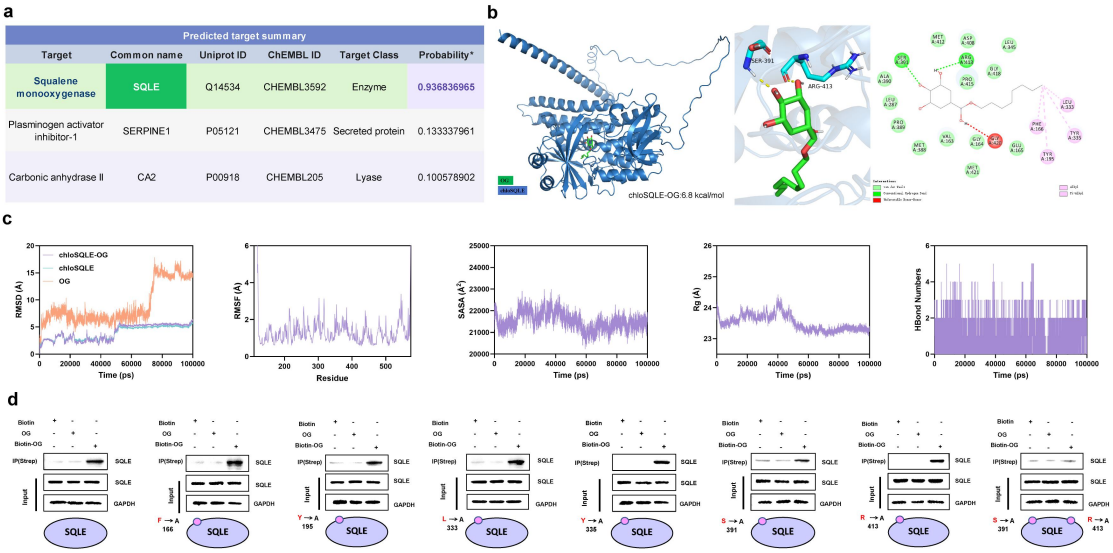

Supplementary Fig.13: OG binds SQLE.

(a) In *silico* target prediction identified cholSQLE as the top candidate target of OG.

(b) Three-dimensional and two-dimensional molecular docking analyses of OG bound to cholSQLE. OG is shown in green and cholSQLE in blue.

(c) MD simulation of the OG–cholSQLE complex over 100 ns, showing RMSD of free OG, cholSQLE, and the complex, together with RMSF, SASA, Rg, and hydrogen-bond numbers.

(d) Pull-down assays with biotinylated OG showing binding to wild-type and mutant cholSQLE proteins (F166A, Y195A, L333A, Y335A, S391A, and R413A), including the S391A/R413A double mutant, to define residues involved in OG binding.

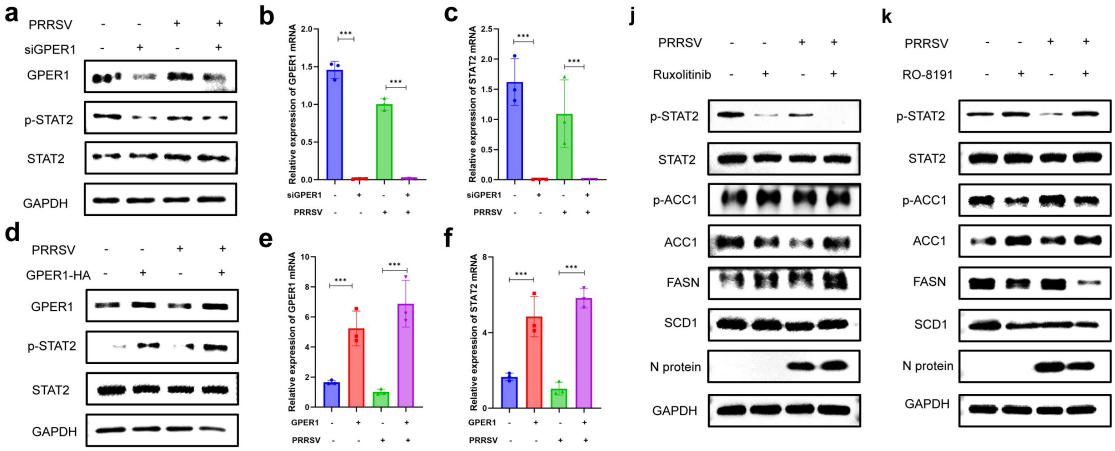

Supplementary Fig.14: JAK-STAT signalling contributes to the GPER1-associated lipid-restrictive response during PRRSV infection

(a-c) GPER1 silencing attenuated STAT2 activation in both uninfected and PRRSV-infected cells. Representative immunoblots show GPER1, p-STAT2 and total STAT2 protein levels (a), with RT-qPCR validation of GPER1 (b) and STAT2 (c) mRNA expression

(d-f) GPER1 overexpression enhanced STAT2 activation in both uninfected and PRRSV-infected cells. Representative immunoblots show GPER1, p-STAT2 and total STAT2 protein levels (d), with RT-qPCR validation of GPER1 (e) and STAT2 (f) mRNA expression.

(j-k) The modulation of JAK-STAT signalling through ruxolitinib-mediated inhibition (j) or RO-8191-mediated activation (k) altered STAT2 phosphorylation, lipogenesis-associated proteins and PRRSV N protein levels. GAPDH served as the loading control.

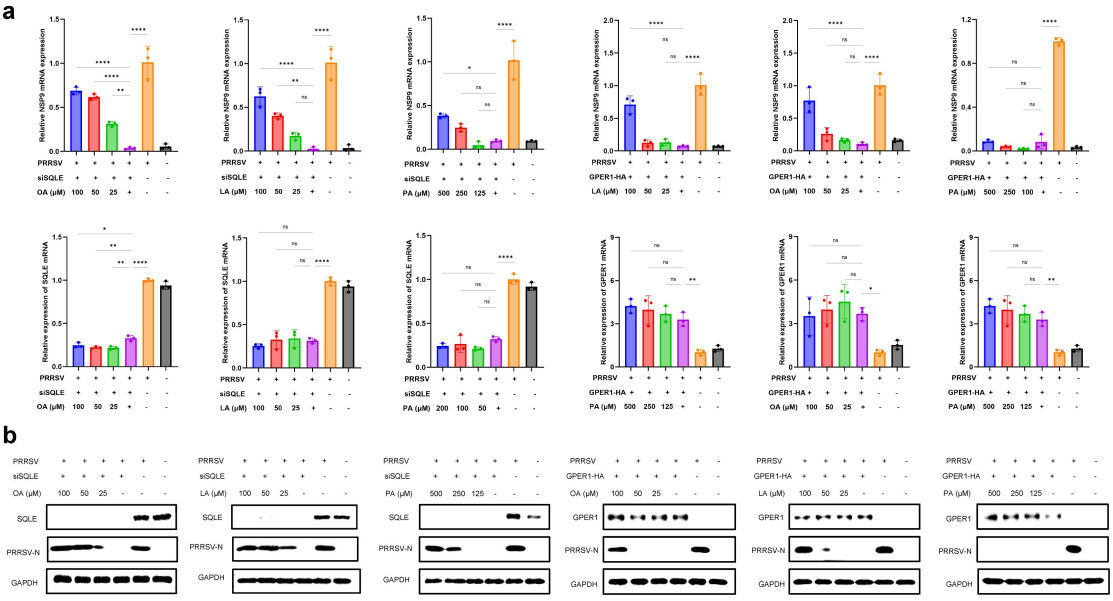

Supplementary Fig.15: SQLE and GPER1 regulate PRRSV replication by modulating fatty acid metabolism.

(a) Exogenous supplementation with OA, LA, or PA at the indicated concentrations reversed the reduction in PRRSV NSP9 mRNA levels caused by SQLE knockdown or GPER1 overexpression in PRRSV-infected MARC-145 cells. SQLE and GPER1 mRNA levels were measured in parallel to confirm the efficiency of SQLE silencing and GPER1 overexpression.

(b) Immunoblot analysis showed that supplementation with OA, LA, or PA similarly restored PRRSV N protein expression suppressed by SQLE knockdown or GPER1 overexpression in infected MARC-145 cells. GAPDH served as a loading control.

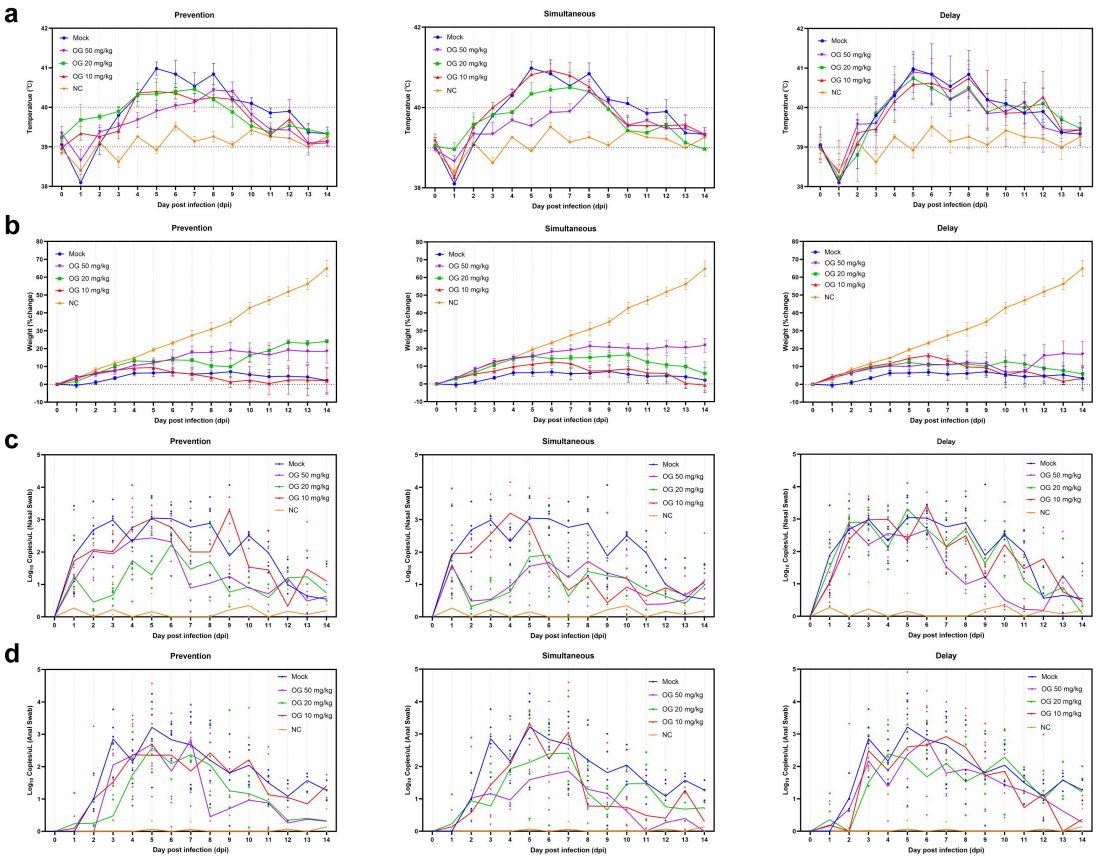

Supplementary Fig.16: Effects of OG on rectal temperature, body weight loss and viral shedding in PRRSV-infected piglets.

(a) Rectal temperature profiles of piglets treated with the indicated doses of OG under prevention, simultaneous and delay regimens. The red dashed line indicates 40 °C, the threshold for fever.

(b) Body-weight changes in piglets over 14 days after PRRSV challenge. Body weight was recorded daily and expressed as the percentage change relative to the baseline value on day 0.

(c and d) Viral shedding kinetics in nasal (c) and anal (d) swabs collected from piglets throughout the experiment under the indicated treatment regimens.

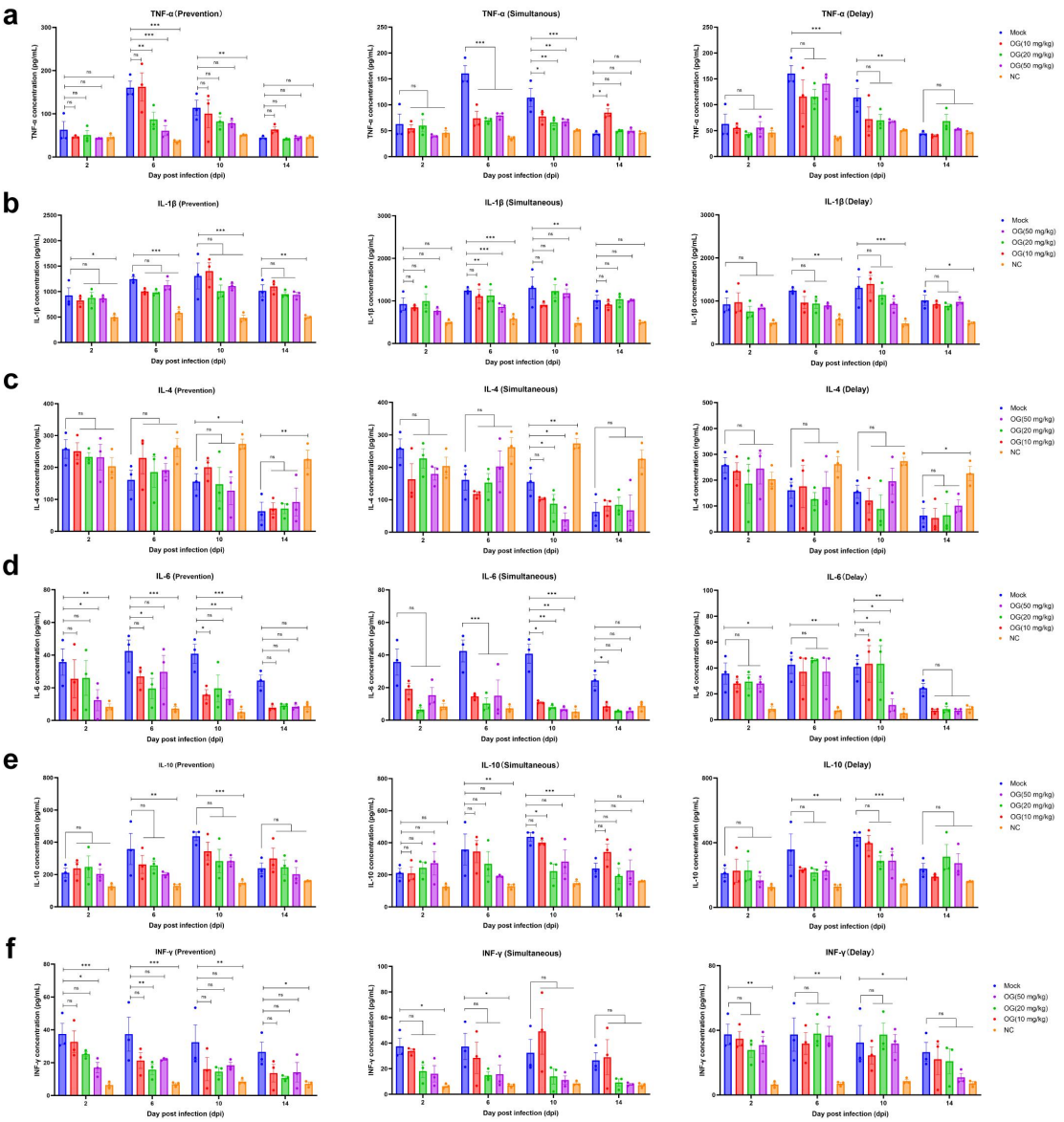

Supplementary Fig.17: Effects of OG treatment on serum cytokine levels in PRRSV-infected piglets.

Serum concentrations of TNF-α **(a)**, IL-1β **(b)**, IL-4 **(c)**, IL-6 **(d)**, IL-10 **(e)** and IFN-γ **(f)** were measured by ELISA in PRRSV-infected piglets treated with the indicated doses of OG under prevention, simultaneous and delay regimens. n = 3 biologically independent serum samples per group; hemolysed serum samples were excluded before analysis.

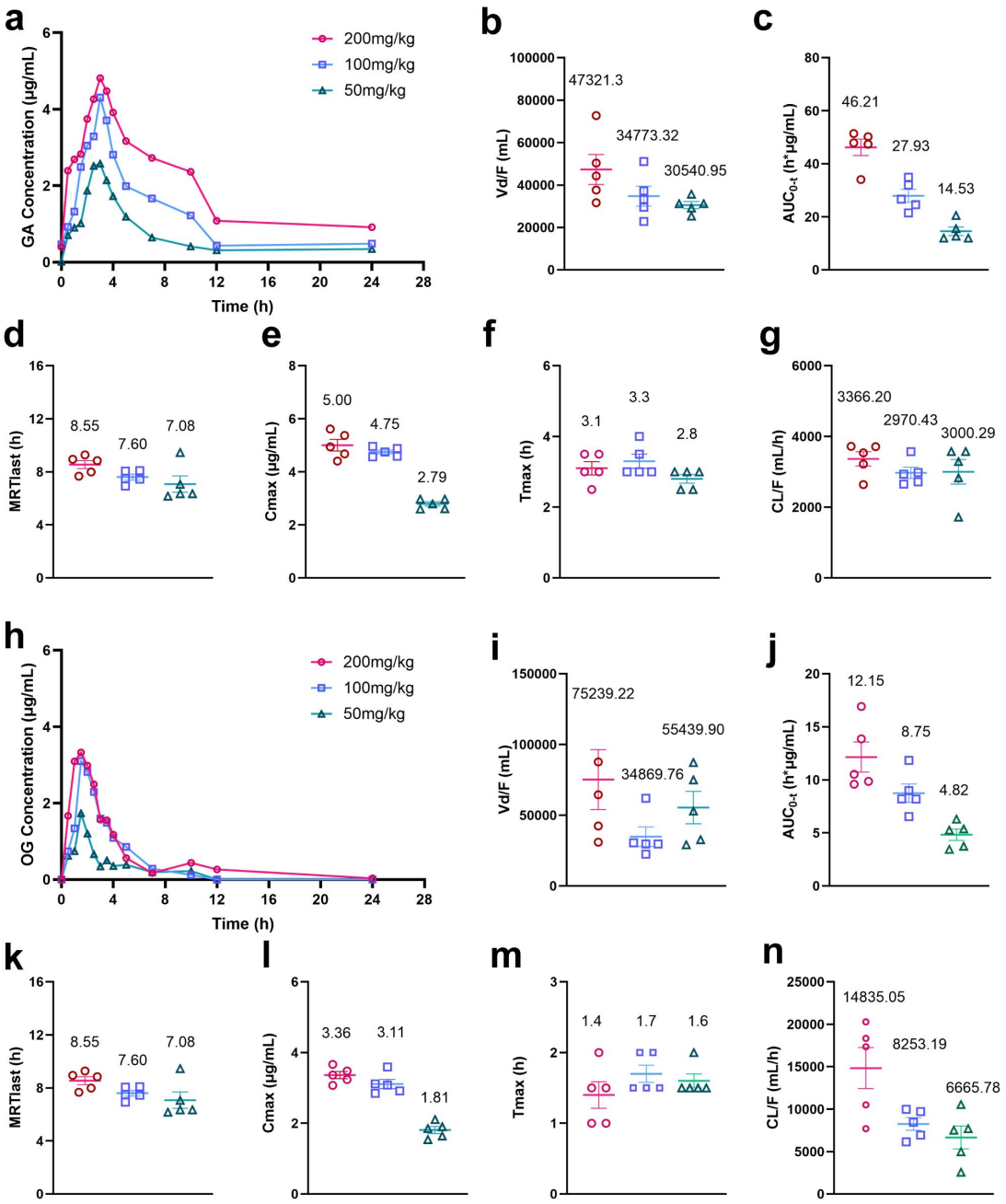

Supplementary Fig. 18: Pharmacokinetic analysis of OG and its metabolite GA in pigs.

(a) Plasma concentration–time profiles of gallic acid (GA) after oral administration of OG at the indicated doses.

(**b-g)** Non-compartmental pharmacokinetic parameters of GA, including apparent volume of distribution (Vd/F) (b), area under the plasma concentration-time curve from time 0 to the last measurable concentration (AUC_{0}–t) (c), mean residence time to the last measurable concentration (MRTlast) (d), maximum plasma concentration (Cmax) (e), time to reach Cmax (Tmax) (f) and apparent clearance (CL/F) (g).

(h) Plasma concentration-time profiles of OG at the indicated doses.

(i–n) Non-compartmental pharmacokinetic parameters of OG, including Vd/F (i), AUC_{0}-t (j), MRTlast (k), Cmax (l), Tmax (m) and CL/F (n).

Pharmacokinetic parameters were calculated by non-compartmental analysis. n = 5 pigs per group.

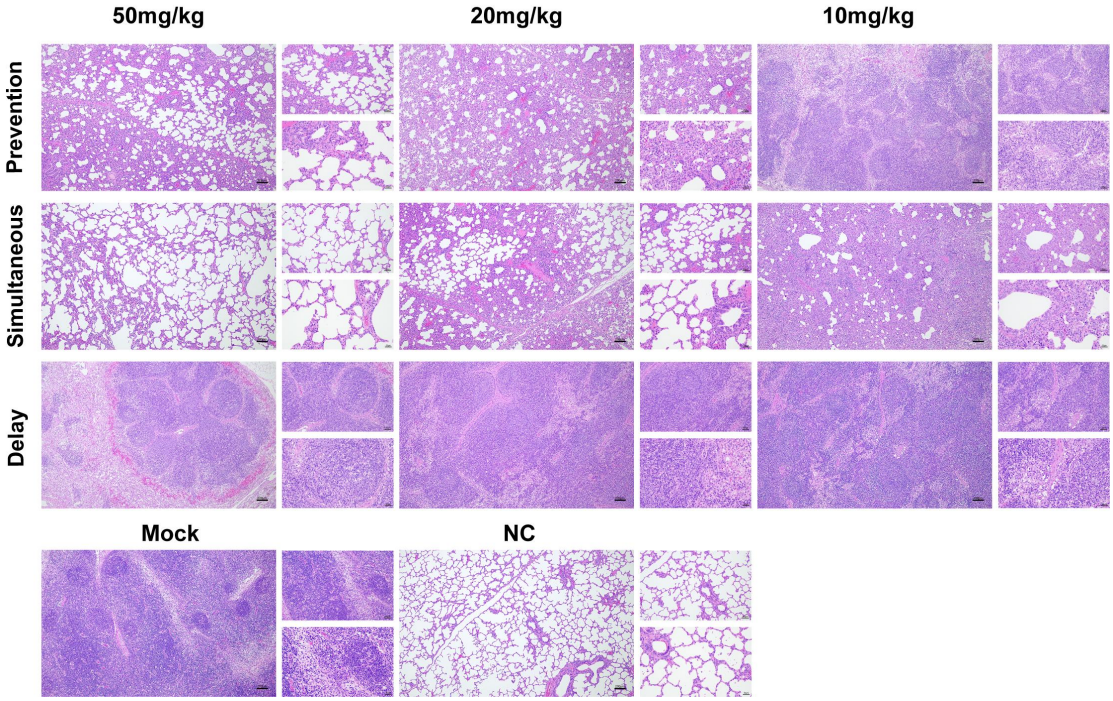

Supplementary Fig. 19： OG treatment alleviates PRRSV-induced histopathological lesions in piglets.

Representative H&E-stained sections of lung and lymphoid tissues collected at 14 dpi. PRRSV challenge induced interstitial pneumonia, alveolar septal thickening, inflammatory cell infiltration and lymphoid tissue lesions, whereas OG treatment reduced these pathological changes. Scale bars are indicated.

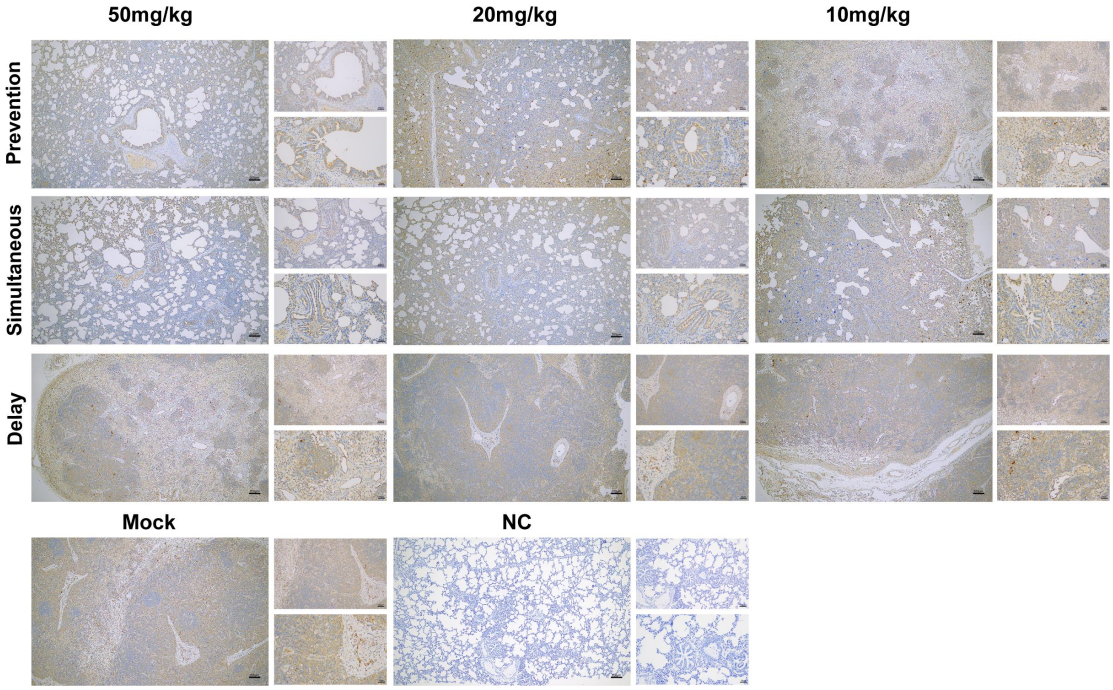

Supplementary Fig. 20：Immunohistochemical detection of PRRSV antigen in lung tissues from OG-treated piglets after PRRSV challenge.

Representative immunohistochemical staining of PRRSV antigen in lung sections from piglets treated with OG at 50, 20 or 10 mg/kg under preventive, simultaneous or delayed dosing regimens. Brown DAB staining indicates PRRSV-positive cells, and nuclei were counterstained with hematoxylin. PRRSV challenge resulted in extensive viral antigen accumulation in lung tissues, whereas OG treatment reduced PRRSV-positive staining to varying degrees, with the most apparent reduction observed in the 50 mg/kg simultaneous-treatment group. Mock and NC groups are shown for comparison. Scale bars are indicated.

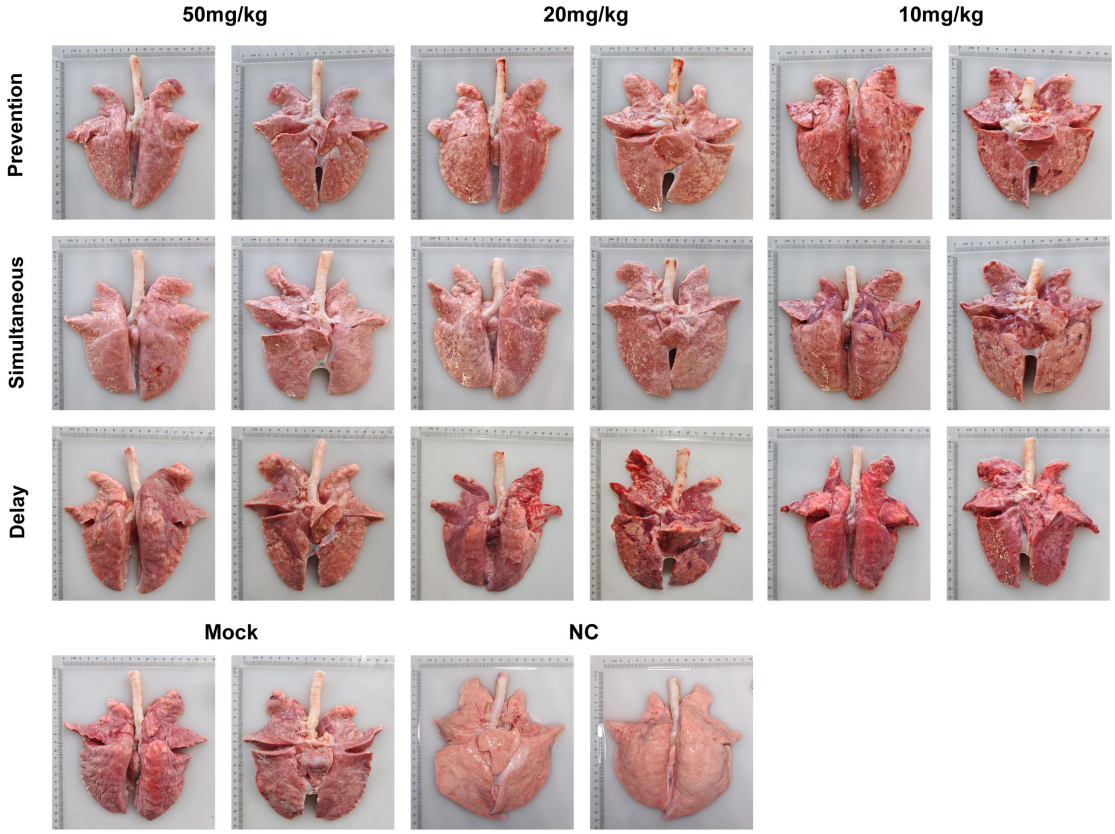

Supplementary Fig. 21：Gross pulmonary lesions following PRRSV challenge and OG treatment. Representative paired ventral and dorsal lung images collected at 14 dpi PRRSV infection caused visible pulmonary lesions, including multifocal consolidation, hemorrhagic discoloration and mottled lung appearance, whereas OG treatment reduced these pathological changes to varying degrees. The most evident protection was observed in the 50 mg/kg simultaneous-treatment group. Mock, uninfected control; NC, PRRSV-challenged untreated control.

Supplementary Table 1 | siRNAs used in this study

Sequences are shown in the 5′–3′ orientation without terminal 3′ dTdT overhangs. All siRNAs contained 3′ dTdT overhangs and were HPLC-purified.

Target	siRNA name	Sense strand (5′–3′)	Antisense strand (5′–3′)
ACC1	siACC1	GCCUCUCCUAGAAUUGCAA	UUGCAAUUCUAGGAGAGGC
FASN	siFASN	GCCGAGUACAAUGUCAACA	UGUUGACAUUGUACUCGGC
SCD1	siSCD1	GGAGACGGAAGCUACAAGA	UCUUGUAGCUUCCGUCUCC
HSL	siHSL	GGCGCAAGUCUCAGAAGAU	AUCUUCUGAGACUUGCGCC
ATGL	siATGL	AGAUGUGCAAGCAGGGCUA	UAGCCCUGCUUGCACAUCU
MGLL	siMGLL	CCACAAAGAGCUUCCUGAA	UUCAGGAAGCUCUUUGUGG
SQLE	siSQLE-1	GCUGUUGCAGUCUAUGCUA	UAGCAUAGACUGCAACAGC
SQLE	siSQLE-2	CGAGUACUUGUUGACGUUA	UAACGUCAACAAGUACUCG
SQLE	siSQLE-3	GAAGAAAGGUGACAGUAAU	AUUACUGUCACCUUUCUUC
GPER1	siGPER1-1	GGCUGUACAUUGAGCAGAA	UUCUGCUCAAUGUACAGCC
GPER1	siGPER1-2	CCGACCUGUACUUCAUCAA	UUGAUGAAGUACAGGUCGG
GPER1	siGPER1-3	GGUUCAGCAGCGCCGUGUA	UACACGGCGCUGCUGAACC

Supplementary Table 2 | Primers used in this study

Primer sequences are shown in the 5′–3′ orientation. The probe used for PRRSV absolute quantification is listed below the table rather than as a separate table column.

Target	Application	Forward primer (5′–3′)	Reverse primer (5′–3′)
GPER1	RT–qPCR	ATGGCTGTGACTTCCCAAGC	CTACACGGCGCTGCTGAACC
SQLE	RT–qPCR	AGTTCGCCCTCTTCTCGGAT	GACTGTCACCTTTCTTCCATC TCT
PPAR	RT–qPCR	TGAGTTCGCTGTGAAGTT	CAATCTGTCTGAGGTCTGT
ACC1	RT–qPCR	TAGTCTGCCACGGATCCAGA	GGGAGGGATCTCTGAGGGTT
FASN	RT–qPCR	CACATCGTTCGAGCAGCATG	AATTTCCAGGAAGCGACCGT
SCD1	RT–qPCR	AGGGCCCCAATGTATGTGTG	AAAGATGTAAGGCACCCGGG
ATGL	RT–qPCR	GAGATGTGCAAGCAGGGCTA	ACTCTCCATGGCCTCATCCT
HSL	RT–qPCR	CCTCCGGGAGTATGTTACGC	ACACCAGCCCAATGGAGATG
MGLL	RT–qPCR	GTCTTCCTTCTGGGCCACTC	GTTGAGCACTTTCGCAGCAA
CPT1A	RT–qPCR	CTGTATGTCCTTCCAACTCA	GATGTGCTTGCTGTCTCT
LPIN1	RT–qPCR	CAAGCAAGTAGGAGTGTCT	GCGGAGGCAGAATGAATA
β-actin	RT–qPCR	CTCCATCATGAAGTGCGACGT	GTGATCTCCTTCTGCATCCTG TC
NSP9	RT–qPCR	CTAAGAGAGGTGGCCTGTCG	GAGACTCGGCATACAGCACA
STAT2	RT–qPCR	ACACCGTGGATGAGGCTTAC	TAGCTTGGAAGGGACACACG
PRRSV (M)	Probe-based RT–qPCR	TTGCTAGGCCGCAAGTAC	ACGCCGGACGACAAATGC

Note: The PRRSV (M) primer pair was used for probe-based absolute quantification. Probe sequence (5′–3′): [FAM-CTGGCCCCTGCCCACCAC-BHQ1].

Supplementary Table 3 | Antibodies used in this study

Antibody	Antibody type	Supplier	Catalogue no.	Application	Dilution
Anti-PRRSV N	Rabbit pAb	GeneTex	GTX129270	WB, IF, IHC	WB, 1:2000; IF, 1:1000; IHC, 1:100
Anti-GPER1	Rabbit pAb	Proteintech	13463-1-AP	WB	WB, 1:1000
Anti-SQLE	Rabbit mAb	Proteintech	12544-1-AP	WB	WB, 1:1000
Anti-GAPDH	Rabbit pAb	Proteintech	10494-1-AP	WB	WB, 1:5000
Anti-phospho-ACC1	Rabbit pAb	Affinity	AF3421	WB	WB, 1:1000
Anti-ACC1	Rabbit pAb	Affinity	AF7864	WB	WB, 1:1000
Anti-FASN	Rabbit pAb	Proteintech	10624-2-AP	WB	WB, 1:1000
Anti-SCD1	Rabbit pAb	Proteintech	28678-1-AP	WB	WB, 1:2000
Anti-phospho-HSL	Rabbit mAb	ABclonal	AP1151	WB	WB, 1:1000
Anti-HSL	Rabbit mAb	ABclonal	A24689	WB	WB, 1:5000
Anti-MGLL	Rabbit mAb	Abcam	ab24701	WB	WB, 1:500
Anti-ATGL	Rabbit mAb	ABclonal	A28710	WB	WB, 1:5000
Anti-STAT2	Rabbit pAb	Affinity	AF6342	WB	WB, 1:1000
Anti-phospho-STAT2	Rabbit pAb	Affinity	AF3342	WB	WB, 1:1000
HRP-conjugated goat anti-rabbit IgG	Goat pAb	Proteintech	SA00001-2	WB	WB, 1:5000
HRP-conjugated goat anti-mouse IgG	Goat pAb	Proteintech	SA00001-1	WB	WB, 1:5000
Alexa Fluor 488-conjugated goat anti-mouse IgG	Goat pAb	Santa Cruz Biotechnology	sc-516640	IF	IF, 1:5000
Anti-HA tag antibody	Rabbit pAb	Proteintech	51064-2-AP	WB	WB, 1:5000
Anti-GST tag antibody	Rabbit pAb	Proteintech	10000-0-AP	WB	WB, 1:5000

Abbreviations: WB, western blotting; IF, immunofluorescence; IHC, immunohistochemistry; pAb, polyclonal antibody; mAb, monoclonal antibody.